

Parotid Gland MRI Segmentation Based on Swin-Unet and Multimodal Images

Yin Dai, Zi'an Xu, Fayu Liu, Siqi Li, Sheng Liu, Lifu Shi, Jun Fu

Abstract—Parotid gland tumors account for approximately 2% to 10% of head and neck tumors. Preoperative tumor localization, differential diagnosis, and subsequent selection of appropriate treatment for parotid gland tumors is critical. However, the relative rarity of these tumors and the highly dispersed tissue types have left an unmet need for a subtle differential diagnosis of such neoplastic lesions based on preoperative radiomics. Recently, deep learning methods have developed rapidly, especially Transformer beats the traditional convolutional neural network in computer vision. Many new Transformer-based networks have been proposed for computer vision tasks. In this study, multicenter multimodal parotid gland MRI images were collected. The Swin-Unet which was based on Transformer was used. MRI images of STIR, T1 and T2 modalities were combined into a three-channel data to train the network. We achieved segmentation of the region of interest for parotid gland and tumor. The DSC of the model on the test set was 88.63%, MPA was 99.31%, MIoU was 83.99%, and HD was 3.04. Then a series of comparison experiments were designed in this paper to further validate the segmentation performance of the algorithm.

Index Terms—Deep learning, Transformer, Parotid gland, Image segmentation, Multimodal images.

I. INTRODUCTION

WORLDWIDE, head and neck tumors (cancer of the lip, oral cavity, salivary glands, pharynx, and larynx) are the eighth most common malignancies with a mortality rate of 40-60% [1], [2]. Parotid gland tumors (PGTs) are a clinically common type of head and neck tumor. It accounts for approximately 2% to 10% of head and neck tumors [3]. Therefore, preoperative tumor localization, differential diagnosis and subsequent selection of appropriate treatment for PGTs is crucial [4], [5]. However, in the latest WHO classification, the relative rarity and highly dispersed tissue types of such tumors leave an unmet need for a subtle differential diagnosis of such neoplastic lesions based on preoperative radiomics [3].

MRI is the first choice of imaging modality for the examination of PGTs. This is because it has the ability to assess patient anatomy without the use of ionizing radiation [6] and has a higher resolution for imaging soft tissues, providing more information about the nature of the tumor and surrounding tissues [7]–[9]. However, manual assessment of parotid status by MRI imaging is a subjective, time-consuming, error-prone process [10] and may produce inconsistent results [11]. Automated image analysis methods offer the possibility of consistent, objective, and rapid diagnosis of parotid tumors [10]. A good, automated method can significantly reduce the amount of time clinicians must spend on this task. However, segmentation of the parotid gland is particularly challenging due to its variable shape and often low contrast with surrounding structures [12].

Automatic segmentation models based on deep learning have been developed rapidly in recent years [13]–[15]. Deep convolution models have been highly successful in biomedical image segmentation and have been introduced to the head and neck anatomy segmentation field [16]. In recent years there are many excellent works that have attempted to implement segmentation of the parotid region using several different deep learning methods [17]–[24]. Recently, Transformer has made a breakthrough in computer vision (CV), and many new Transformer-based methods for CV tasks have been proposed [25]. One of them is Swin-Unet, a Transformer-based segmentation network that performs well on CT images of the liver [26]. Considering the difficulty of parotid segmentation, we implemented a Swin-Unet-based method to segment the region of interest (ROI) of parotid gland and tumor, and designed several comparative experiments to verify the effectiveness of the method in this paper.

The rest of this paper is organized as follows. Section II describes some work that is closely related to this paper. Section III describes the specific methods of preparation. Section IV presents the experiments and results, and the results are discussed. Finally, a summary of our work is presented in Section V.

II. RELATED WORK

A. U-Net, the classical U-shaped structured segmentation network

U-Net [27] as a classical segmentation network, whose symmetric U-shaped structure has a profound influence on the subsequent network design. Until now, numerous segmentation network papers still use U-Net as a comparison experiment to evaluate the effectiveness of the network.

FCN [28] was the first to solve the semantic segmentation problem by replacing the last fully connected layer of a traditional classification network with a convolutional layer for up-sampling. However, since the decoder of FCN is relatively simple compared to the encoder, it is slightly lacking in the details of segmentation. U-Net has made major changes in the decoder. U-Net uses multiple layers of convolution and up-sampling so that it is symmetric with the encoder structure. U-Net also uses jump connections to fuse high-resolution features from the encoder at different scales to mitigate the loss of spatial information due to down-sampling. These improvements have led to a significant improvement in the segmentation effect. And such a classical U-shaped structure also inspired the subsequent research, and various new U-shaped structure networks were proposed later.

In summary, U-Net goes beyond proposing a simple network and pioneers a new U-shaped segmented network architecture. The backbone of U-Net can be replaced by classical classification networks such as VGG [29] or ResNet [30] to obtain different U-Net networks. The Swin-Unet used in this paper is obtained by turning the backbone into Swin Transformer.

B. Swin Transformer, a CV network based on Attention mechanism

The Attention mechanism was first widely used in the field of Natural Language Processing (NLP). It simulates the attention model of the human brain. When people look at a thing in detail, they focus more attention on the more important parts. The Attention mechanism can then simulate this process by assigning higher weights to the more important parts of the network. The Attention mechanism has many different implementations, and one of them is the Multi-Head Attention mechanism. The Transformer [31] based on this mechanism has been very successful on various NLP tasks.

Vision Transformer (ViT) [32] applies Transformer to image classification tasks. Although Transformer lacks inductive bias compared to Convolutional Neural Network (CNN), when pre-trained with a large enough dataset, ViT which uses transfer learning still outperforms CNN.

However, ViT directly splits the image into 16×16 independent patches on one channel, making there is a lack of information passing between these patches. To solve this problem, Swin Transformer [33] introduces shifted windows. The original patches are in separate windows from each other. In the next step the windows will be moved and the new window will contain parts of the original windows, so that the information between the patches can be communicated. This further enhances the capability of Transformer for image classification tasks.

C. Swin-Unet, a segmentation network based on U-Net and Swin Transformer

By replacing the backbone in U-Net with Swin Transformer and making some detail changes, the Swin-Unet [26] is obtained. Swin-Unet is the first U-architecture segmentation network based entirely on Transformer, which consists of an encoder, a bottleneck, a decoder and jump connections. Swin-Unet uses Swin Transformer layer for feature extraction, Patch Merging layer and Patch Expanding layer for down-sampling and up-sampling, and introduces jump links for fusing encoder features in the decoder with reference to U-Net.

The paper proposing Swin-Unet uses the Synapse multi-organ CT dataset to demonstrate that the network works better for medical images. Therefore, in this paper, we designed an experiment of parotid gland segmentation based on Swin-Unet and obtained good experimental results. The specific method will be described in Section III.

III. PROPOSED METHOD

A. Collected Dataset

For imaging data, the dataset collected in this study contains multicenter multimodal MRI images of 148 patients

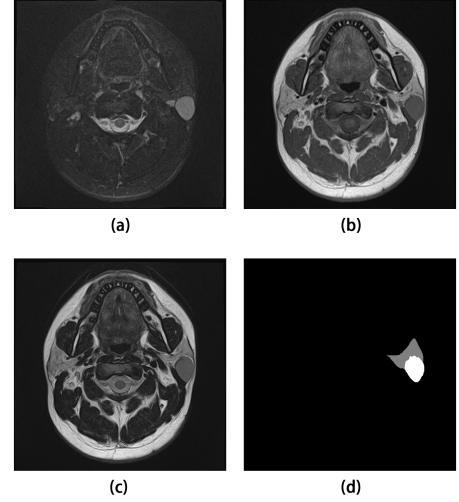


Fig. 1. One-layer slice from an MRI image; (a) STIR image; (b) T1 image; (c) T2 image; (d) Segmentation labels, where the gray area is the parotid gland, and the white area is the tumor.

with parotid gland tumors. The data set is from two centers with different imaging equipment and slice thicknesses. The dataset contains MRI imaging sequences of three modalities, which are short time inversion recovery (STIR), T1-weighted sequence (T1) and T2-weighted sequence (T2), as shown in Figure Fig. 1(a), Fig. 1(b) and Fig. 1(c), respectively.

For the segmentation label, there is a parotid gland on each side of the image. The side with the tumor was selected by experienced clinicians, and the ROI of the parotid gland and tumor were outlined separately as segmentation labels, as shown in Fig. 1(d).

After screening, a total of 1897 MRI image slices were finally available. There were 795 image slices from the first center and 1102 image slices from the second center. In all subsequent experiments, 80% of the used dataset was taken as the training set and the remaining 20% as the test set.

B. Method Overview

As mentioned in Section I, the segmentation of the parotid gland is a very challenging task. And the recently proposed Transformer and its variants have shown excellent performance in natural images and other medical images. Therefore, the network used in this experiment is mainly based on the Swin-Unet introduced in Section II. The structure of the network is shown in Fig. 2.

In this paper, we take advantage of the multimodal STIR, T1 and T2 images from the collected MRI parotid dataset and the network structure of Swin-Unet itself, which requires a three-channel input. Each part of the network will be described in detail in turn.

C. Network Inputs

In the original paper that proposed Swin-Unet, the dataset used was the Synapse multi-organ CT. The CT images of a single layer in the dataset are single-channel grayscale images.

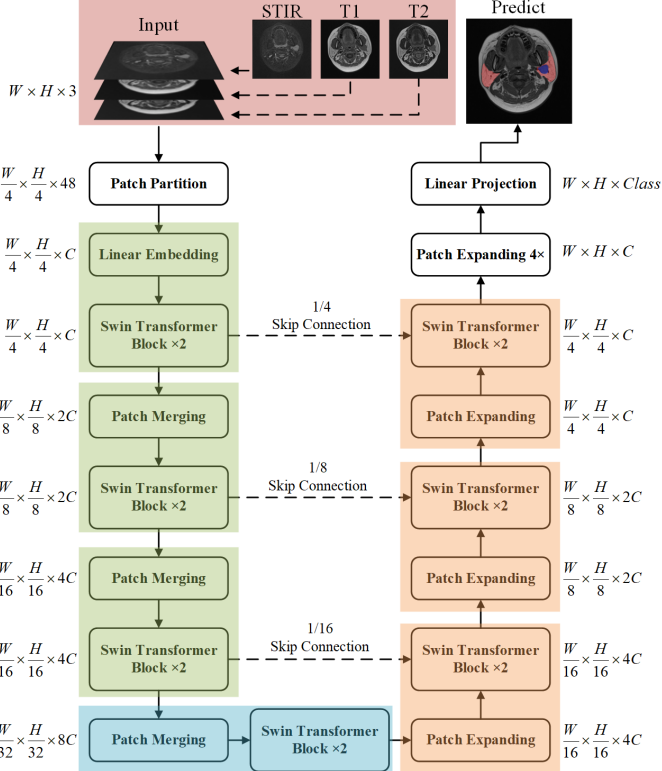


Fig. 2. Network structure diagram.

In contrast, the input images for Swin Transformer's pre-trained model on the ImageNet dataset are three-channel. To be able to use the pre-trained model for transfer learning, the approach of the original Swin-Unet paper was to make three copies of a single-channel CT image to form a three-channel image, which was then fed into the network. Although this does not lead to an increase in information in terms of input. Instead, it increases the memory overhead. But Transformer does not have the inductive bias that CNN has. Therefore, in the case of inadequate datasets, especially for dealing with small data sets like medical images, using models pre-trained with big data for transfer learning is a necessary practice. Otherwise, the final training result of Transformer may not even be as good as traditional CNN.

In summary, using Swin Transformer's pre-trained weights on Swin-Unet's encoder for transfer learning is necessary. And the parotid data set collected in this study contains three different imaging modalities, namely STIR, T1 and T2. Therefore, we innovatively extracted the same slice from the MRI image sequences obtained from the three imaging modalities and stitched them in the channel dimension to form a three-channel image. This enables both using the pre-trained model for transfer learning and inputting more image information to further improve the accuracy of the model. Although the pre-trained model originally used natural images with R, G, and B channels, which are very different in physical sense from the STIR, T1, and T2 channels we use now. However, the comparison experiments designed in Section IV prove that doing so does improve the network partitioning performance.

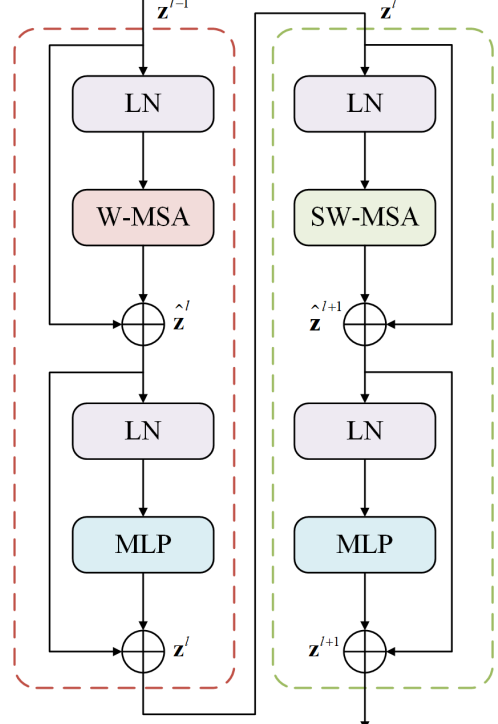


Fig. 3. Swin Transformer structure diagram.

D. Patch Partition layer and Linear Embedding layer

Transformer was first applied in the field of NLP. To improve the speed of network computing, One-Hot encoding is often used to represent each word. However, each different word should correspond to a different One-Hot encoding will result in too large a feature dimension of the input. Therefore, it is necessary to use Embedding layers with learnable parameters for dimensionality reduction.

To use Transformer in the field of CV, it is proposed in ViT to slice an image into 16×16 independent patches and treat the image as 16×16 numbers of words input to the network. The purpose of the Patch Partition layer is to divide the image into several separate patches. In Swin-Unet used in this paper, the Patch Partition layer partitions the input of size $(H, W, 3)$ into patches of size $(\frac{W}{4}, \frac{H}{4}, 48)$. The latter also follows the steps of NLP, using Linear Embedding layers with learnable parameters for dimensionality reduction. In terms of the specific implementation, these two layers can be implemented in one step using a convolution operation with a convolution kernel size of 4×4 and a step size of 4.

E. Swin Transformer layer

As the main feature extraction layer, Swin Transformer consists of two different Attention modules. They are the Window Multihead Self-Attention Module (W-MSA) and the Moving Window Multihead Self-Attention Module (SW-MSA), respectively. The structure of the Swin Transformer is shown in Fig. 3.

The equations for variables \hat{z}^l , z^l , \hat{z}^{l+1} and z^{l+1} in the above figure are shown in equations (1), (2), (3) and (4), respectively.

$$\hat{\mathbf{z}}^l = \mathbf{W} - \text{MSA}(\text{LN}(\mathbf{z}^{l-1})) + \mathbf{z}^{l-1} \quad (1)$$

$$\mathbf{z}^l = \text{MLP}(\text{LN}(\hat{\mathbf{z}}^l)) + \hat{\mathbf{z}}^l \quad (2)$$

$$\hat{\mathbf{z}}^{l+1} = \text{SW-MSA}(\text{LN}(\mathbf{z}^l)) + \mathbf{z}^l \quad (3)$$

$$\mathbf{z}^{l+1} = \text{MLP}(\text{LN}(\hat{\mathbf{z}}^{l+1})) + \hat{\mathbf{z}}^{l+1} \quad (4)$$

In a Swin Transformer Block, the input data goes through the LayerNorm (LN) layer first. The LN here plays a similar role to the BatchNorm (BN), which is commonly used in the CV field. Both are designed to normalize the activation values of the output of the previous layer to avoid the gradient disappearance problem to some extent. The difference between LN and BN is the different dimensionality of the computed normalization. LN is computed in Layer dimension, while BN is computed in Batch dimension. In the NLP field, the batch size of the network is usually smaller than that in the CV field, which makes BN often less effective than LN [34]. Therefore the LN layer is used in Transformer. The formula for LN is shown in equation (5).

$$y = \frac{x - \text{E}[x]}{\sqrt{\text{Var}[x] + \epsilon}} * \gamma + \beta \quad (5)$$

Where $\text{E}[x]$ represents the mean of x , $\text{Var}[x]$ represents the variance of x , ϵ is a very small number to avoid the possibility of a zero denominator, γ and β are learnable parameters.

After going through the LN layer, it is entered into the W-MSA layer or SW-MSA layer. Compared to the multi-headed self-attention (MSA), W-MSA will save much computation for calculating each window separately [33]. For an input image of size (h, w) , assuming that each window contains $M \times M$ patches, the computational complexity formulas for MSA and W-MSA are shown in equations (6) and (7), respectively.

$$\Omega(\text{MSA}) = 4hwC^2 + 2(hw)^2C \quad (6)$$

$$\Omega(\text{W-MSA}) = 4hwC^2 + 2M^2hwC \quad (7)$$

W-MSA can reduce the amount of computation, but it leads to the lack of information communication between the windows. To solve this problem, SW-MSA must be calculated in the later blocks. By moving the window down and right by half the window size and calculating W-MSA again for the moved window, it can realize the information communication between the windows. Therefore, W-MSA and SW-MSA need to appear in pairs. It is also for this reason that the number of Blocks in Swin Transformer is usually even. In Swin-Unet, the number of blocks of Swin Transformer are both 2, which contains one W-MSA block and one SW-MSA block.

After passing through the W-MSA layer or SW-MSA layer, then a BN layer, and finally a Multilayer Perceptron (MLP) for feature mapping, the final output is obtained. And to better solve the gradient vanishing problem, Swin Transformer adds residual links.

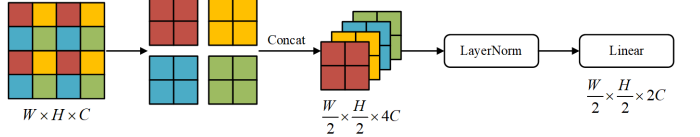


Fig. 4. Patch Merging structure diagram.

F. Patch Merging layer and Patch Expanding layer

Since the Swin Transformer layer does not result in a change in image size, the network requires a down-sampling layer and an up-sampling layer. The down-sampling and up-sampling layers in Swin-Unet are the Patch Merging layer and the Patch Expanding layer, respectively. The structure of the Patch Merging layer is shown in Fig. 4.

Patch Merging is done by first splitting the image into regions of size 4×4 , and pixels in the same position in each region are combined to form a new patch. Connecting these patches in the channel dimension, which will change the size of the input image from (W, H, C) to $(\frac{W}{2}, \frac{H}{2}, 4C)$. Now the number of channels of the image becomes four times the original. However, in U-Net, each Stage will only change the number of channels of the image to twice the original number. Therefore, the number of channels needs to be halved at the end using a linear layer. To avoid the gradient vanishing problem to some extent, another LN layer is added before the linear layer, so that the whole Patch Merging layer is obtained.

The Patch Expanding layer has the opposite effect of the Patch Merging layer. It requires doubling the length and width of the image and halving the number of channels. In contrast, Patch Expanding is relatively simple. The number of channels of the input image is first doubled by a linear layer and then just rearranged. Also, to counteract gradient disappearance, an LN layer is added at the end.

G. Skip Connection

The skip connection allows features from the encoder to be fed into the decoder, thus allowing the decoder to fuse high-resolution features from the encoder at different scales to mitigate the loss of spatial information due to down-sampling. There are different ways of implementing skip connections. In FCN, a point-by-point summation method is used to sum the corresponding pixel values of the feature array directly. While, in U-Net, two feature arrays are concatenated in the channel dimension.

In Swin-Unet, skip connections are used in a slightly different way than in U-Net. After concatenating the two feature arrays in the channel dimension, an additional linear layer is required to halve the number of channels, which is required to comply with the input requirements of the next Swin Transformer layer.

H. Training parameters

In this study, Swin-Unet was used to implement the segmentation of the ROI of parotid gland and tumor in MRI images. Three categories of segmentation results were set up for the network, which are background, parotid gland, and

tumor. This paper investigates the medical image segmentation problem, so the classical cross-entropy function is used as the loss function. Set the batch size to 8 and the optimizer used is AdamW. The learning rate was 0.0001 and the decay rate of learning rate was 0.05. 20 epochs were trained using a transfer learning method, and the pre-training weights of the encoder part used the model parameters of the tiny version of Swin Transformer on ImageNet. The network finally achieves better training results. The test results and evaluation metrics of the model will be shown in Section IV.

IV. EXPERIMENTS AND DISCUSSION

In this section, we first show the experimental results of the segmentation model obtained by training according to the method given in Section III. We then designed four different sets of comparison experiments and made a corresponding discussion based on the results of these experiments.

A. Experimental results of the segmentation model

Following the training method and parameters given in Section III, after network training the segmentation model was obtained. We used four segmentation evaluation metrics to evaluate the segmentation effectiveness of the model on the test set, which are Dice-Similarity coefficient (DSC), Mean Pixel Accuracy (MPA), Mean Intersection over Union (MIoU), and Hausdorff Distance (HD).

The equations for Dice, MPA and MIoU are shown in equations (8), (9) and (10), respectively. In the formula, TP is the number of pixels correctly assigned to the category, FP is the number of pixels incorrectly assigned to the category, TN is the number of pixels correctly assigned to other categories, and FN is the number of pixels incorrectly assigned to other categories. DSC, MPA and MIoU reflect the area accuracy of the segmentation results, and higher values prove better results.

$$\text{Dice} = \frac{2TP}{FP + 2TP + FN} \quad (8)$$

$$MPA = \frac{TP + TN}{FN + TP + FP + TN} \quad (9)$$

$$MIoU = \frac{TP}{FN + TP + FP} \quad (10)$$

The equation of HD is shown in equation (11), where the equations of $h(A, B)$ and $h(B, A)$ are shown in equations (12) and (13), respectively.

$$H(A, B) = \max(h(A, B), h(B, A)) \quad (11)$$

$$h(A, B) = \max(a \in A) \min(b \in B) \quad \|a - b\| \quad (12)$$

$$h(B, A) = \max(b \in B) \min(a \in A) \quad \|b - a\| \quad (13)$$

The DSC on the model test set was 88.63%, MPA was 99.31%, MIoU was 83.99%, and HD was 3.04. A visual image of the partial test set segmentation results compared

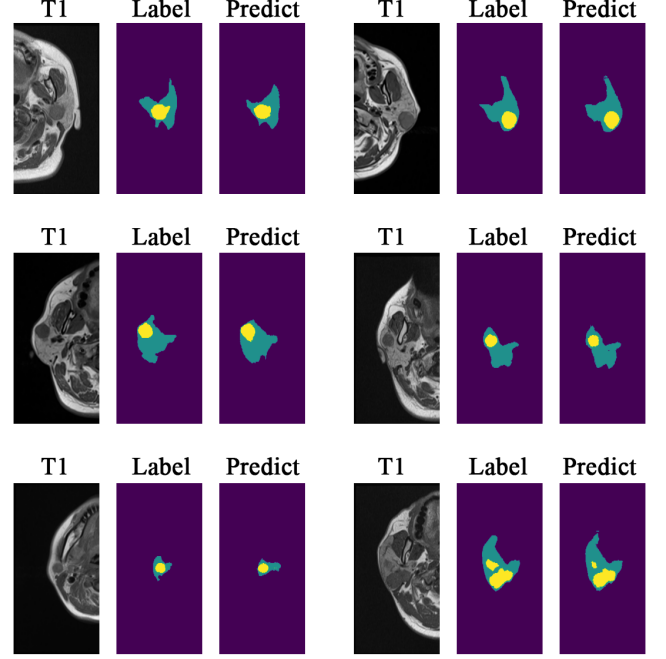


Fig. 5. Visual images of the segmentation results of the partial test set compared with the segmentation labels. The three images of each set from left to right are: the T1 image, the manually outlined labels and the prediction results of the segmentation model.

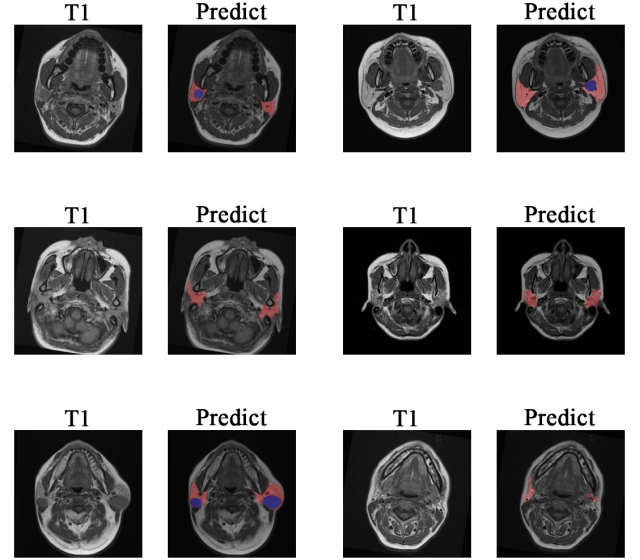


Fig. 6. Visualization images of partial test set segmentation results overlayed on T1. In each set of two images, the left one is the T1 image and the right one is the prediction result of the segmentation model.

with the segmentation labels is shown in Fig. 5. The visualized image of partial test set segmentation results superimposed on the T1 image is shown in Fig. 6. The model has a better overall segmentation effect. However, due to the complex tissue structure of the head and neck MRI, the model still has some room for improvement in the segmentation results of slices containing smaller areas of the parotid gland.

TABLE I
VALUES OF THE FOUR EVALUATION INDICATORS
FOR THE NINE NETWORK MODELS.

Model	DSC(%)	MPA(%)	MIoU(%)	HD
U-Net	87.83	99.25	83.01	3.09
UNet++	87.73	99.28	83.14	3.11
MANet	86.52	99.15	81.34	3.23
LinkNet	86.90	99.26	82.04	3.12
PSPNet	84.70	98.99	79.18	3.38
PAN	83.71	98.98	78.27	3.42
DeepLabV3	86.49	99.17	81.30	3.21
DeepLabV3+	87.54	99.19	82.43	3.10
Swin-Unet	88.63	99.31	83.99	3.04

TABLE II
RESULTS OF IMAGE TRAINING USING STIR, T1, AND T2 CHANNELS
VERSUS USING ONLY ONE OF THE MODALITIES.

Channel	DSC(%)	MPA(%)	MIoU(%)	HD
(STIR, STIR, STIR)	76.22	98.72	71.30	3.76
(T1, T1, T1)	79.80	99.05	74.45	3.46
(T2, T2, T2)	83.50	99.09	78.18	3.37
(STIR, T1, T2)	88.63	99.31	83.99	3.04

B. Comparison of Swin-Unet-based and other conventional network-based model segmentation experiments

To prove that the Swin-Unet can achieve the best results on the dataset, we trained nine classical deep learning segmentation networks including Swin-Unet using the same data, and the other eight are U-Net [27], UNet++ [35], MA-Net [36], LinkNet [37], PSPNet [38], PAN [39], DeepLabV3 [40], and DeepLabV3+ [41].

We use the same four evaluation metrics to quantify the performance of these segmentation network models. The evaluation metric values for the nine network models are shown in TABLE I. From the results of the tests, Swin-Unet was ahead of other traditional networks in all metrics.

C. Comparison experiment of training with STIR, T1 and T2 channels versus training with only one channel of them

In this paper, we innovatively input the three different modalities of STIR, T1 and T2 data into Swin-Unet as a single image with three channels. To quantify the performance gains from doing so and to demonstrate that the performance gains are not the result of either modality acting alone, we designed comparative experiments with networks trained using only one type of modal images.

In this experiment, the control group used three modalities, STIR, T1, and T2, as the three-channel input network of the images. The three experimental groups took one of these three modalities in turn and made three copies as the three-channel image input network. Both experimental and control groups used transfer learning. The results of the model on the test set were evaluated and compared by continuing to use the four evaluation metrics from the previous experiment, and the results of the experiment are shown in TABLE II.

In all four metrics, the results using the STIR, T1, and T2 channels showed a greater performance improvement than the results using images from any one of these modalities alone.

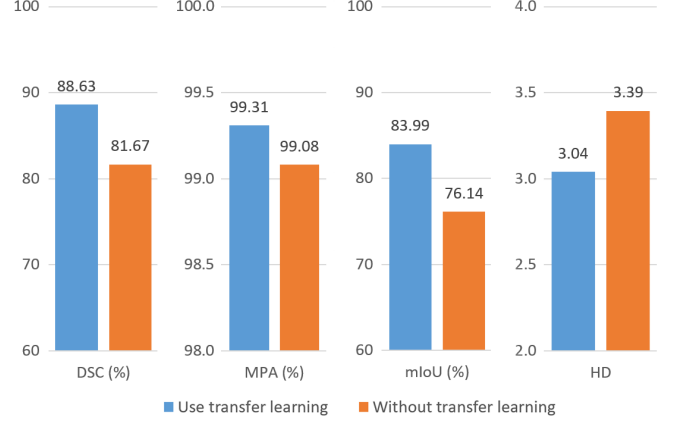


Fig. 7. Results of using transfer learning and without transfer learning.

This proves that using STIR, T1, and T2 modalities as a three-channel input network for images does lead to better results.

D. Comparison experiments using transfer learning versus without transfer learning

In the previous comparison experiment, it was shown that combining STIR, T1, and T2 modalities as a three-channel image input network can achieve better performance. However, Swin Transformer's pre-trained model is based on natural images trained in ImageNet with R, G and B as the three channels. After the input data triple channel changes from R, G and B to STIR, T1 and T2, can transfer learning still have a positive effect on the performance of the model?

To verify this question, we design a comparison experiment using transfer learning versus without transfer learning in this paper. In this experiment, the initialization weights used by the group using transfer learning were tiny versions of Swin Transformer's pre-trained model on ImageNet. The weights of the group without transfer learning are then randomly generated by the algorithm. The experimental results are shown in Fig. 7.

The results show that although the input data three channels change from R, G, and B to STIR, T1, and T2, using transfer learning still improves the performance. This may be because the Transformer-based Swin-Unet lacks some inductive bias that CNN have. For example, CNN considers image information as having spatial locality, and reduces the parameter space by sliding convolution and sharing weights. This also allows the CNN to have the generalizability of the object in terms of image location. Such a priori knowledge is what Transformer lacks. The use of transfer learning can precisely compensate for the lack of inductive bias of Transformer by pre-training with big data, and may obtain more common higher-order image features. Therefore, after the reasonable use of transfer learning, the performance of the model is better than without transfer learning, even better than CNN.

TABLE III
RESULTS FOR THE FOUR CONTROL GROUPS
AND ONE EXPERIMENTAL GROUP.

Experiment group	DSC(%)	MPA(%)	MIoU(%)	HD
train, test: random	88.63	99.31	83.99	3.04
train: 1, test: 1	86.12	99.19	80.64	3.33
train: 1, test: 2	79.62	98.92	73.95	3.68
train: 2, test: 1	80.14	98.64	74.18	3.81
train: 2, test: 2	89.45	99.34	84.94	3.06

E. Comparison experiment of the difference between different center images

The dataset collected in this study contains two sets of images from different centers. The two sets of images differed in terms of imaging equipment and slice thickness. The practice in previous experiments was to first mix the two sets of images and then randomly select the training and test sets from them. To verify the rationality of doing so, this experiment used the above approach as a control group and designed four experimental groups with different training and test sets from each other. They are, in order, the training set using the first central image and the test set using the first central image, the training set using the first central image and the test set using the second central image, the training set using the second central image and the test set using the first central image, and the training set using the second central image and the test set using the second central image.

The same four segmentation metrics were used to evaluate the model performance, and the results of the metrics for each of the four experimental groups and one control group are shown in TABLE III.

We find that the evaluation metrics of the model are similar to the control group when the data in the training and test sets are from the same center, and the evaluation metrics of the model and will be very different from the experimental group when the data in the training and test sets are from different centers.

Therefore, it can be concluded that data from different centers have great differences in deep learning. The training set of the network should contain data from multiple centers so that the trained model can maintain high accuracy on data from different centers.

V. CONCLUSION

In this paper, based on Swin-Unet, three imaging modalities STIR, T1 and T2 of MRI are innovatively used as the three-channel input of the network, and a parotid segmentation model with better performance is trained. On the test set the model has a DSC of 88.63%, MPA of 99.31%, MIoU of 83.99%, and HD of 3.04.

We designed four different sets of comparison experiments, which proved the following conclusions. Swin-Unet has better segmentation results than the traditional network on this dataset. Using STIR, T1, and T2 modalities as a three-channel input network is better than replicating only one of them for three channels. Transfer learning can improve model segmentation performance. The training set should contain images from all centers in the dataset.

REFERENCES

- [1] H. Sung, J. Ferlay, R. L. Siegel, M. Laversanne, I. Soerjomataram, A. Jemal, and F. Bray, "Global cancer statistics 2020: Globocan estimates of incidence and mortality worldwide for 36 cancers in 185 countries," *CA: a cancer journal for clinicians*, vol. 71, no. 3, pp. 209–249, 2021. I
- [2] Y. Liu, Y. Lei, Y. Fu, T. Wang, J. Zhou, X. Jiang, M. McDonald, J. J. Beitler, W. J. Curran, T. Liu *et al.*, "Head and neck multi-organ auto-segmentation on ct images aided by synthetic mri," *Medical Physics*, vol. 47, no. 9, pp. 4294–4302, 2020. I
- [3] R. R. Seethala and G. Stenman, "Update from the 4th edition of the world health organization classification of head and neck tumours: tumors of the salivary gland," *Head and neck pathology*, vol. 11, no. 1, pp. 55–67, 2017. I
- [4] N. Tong, S. Gou, S. Yang, M. Cao, and K. Sheng, "Shape constrained fully convolutional densenet with adversarial training for multiorgan segmentation on head and neck ct and low-field mr images," *Medical physics*, vol. 46, no. 6, pp. 2669–2682, 2019. I
- [5] E. Gündüz, Ö. F. Alçin, A. Kızılıy, and C. Piazza, "Radiomics and deep learning approach to the differential diagnosis of parotid gland tumors," *Current Opinion in Otolaryngology & Head and Neck Surgery*, vol. 30, no. 2, pp. 107–113, 2022. I
- [6] C. E. Cardenas, A. S. Mohamed, J. Yang, M. Gooding, H. Veeraraghavan, J. Kalpathy-Cramer, S. P. Ng, Y. Ding, J. Wang, S. Y. Lai *et al.*, "Head and neck cancer patient images for determining auto-segmentation accuracy in t2-weighted magnetic resonance imaging through expert manual segmentations," *Medical physics*, vol. 47, no. 5, pp. 2317–2322, 2020. I
- [7] E. C. Kuan, J. M.-S. Clair, and M. A. S. John, "Evaluation of parotid lesions," *Otolaryngologic Clinics of North America*, vol. 49, no. 2, pp. 313–325, 2016. I
- [8] A. Christe, C. Waldherr, R. Hallett, P. Zbären, and H. Thoeny, "Mr imaging of parotid tumors: typical lesion characteristics in mr imaging improve discrimination between benign and malignant disease," *American journal of neuroradiology*, vol. 32, no. 7, pp. 1202–1207, 2011. I
- [9] D. Močnik, B. Ibragimov, L. Xing, P. Strojan, B. Likar, F. Pernuš, and T. Vrtovec, "Segmentation of parotid glands from registered ct and mr images," *Physica Medica*, vol. 52, pp. 33–41, 2018. I
- [10] A. B. Slama, Z. Mbarki, H. Seddik, J. Marrakchi, S. Boukriba, and S. Labidi, "Improving parotid gland tumor segmentation and classification using geometric active contour model and deep neural network framework," *Traitemet du Signal*, vol. 38, no. 4, 2021. I
- [11] N. Tong, S. Gou, S. Yang, D. Ruan, and K. Sheng, "Fully automatic multi-organ segmentation for head and neck cancer radiotherapy using shape representation model constrained fully convolutional neural networks," *Medical physics*, vol. 45, no. 10, pp. 4558–4567, 2018. I
- [12] A. Hänsch, M. Schwier, T. Gass, T. Morgas, B. Haas, J. Klein, and H. K. Hahn, "Comparison of different deep learning approaches for parotid gland segmentation from ct images," in *Medical Imaging 2018: Computer-Aided Diagnosis*, vol. 10575. International Society for Optics and Photonics, 2018, p. 1057519. I
- [13] M. Kosmin, J. Ledsam, B. Romera-Paredes, R. Mendes, S. Moinuddin, D. de Souza, L. Gunn, C. Kelly, C. Hughes, A. Karthikesalingam *et al.*, "Rapid advances in auto-segmentation of organs at risk and target volumes in head and neck cancer," *Radiotherapy and Oncology*, vol. 135, pp. 130–140, 2019. I
- [14] C. E. Cardenas, J. Yang, B. M. Anderson, L. E. Court, and K. B. Brock, "Advances in auto-segmentation," in *Seminars in radiation oncology*, vol. 29, no. 3. Elsevier, 2019, pp. 185–197. I
- [15] S. Zhang, H. Wang, S. Tian, X. Zhang, J. Li, R. Lei, M. Gao, C. Liu, L. Yang, X. Bi *et al.*, "A slice classification model-facilitated 3d encoder-decoder network for segmenting organs at risk in head and neck cancer," *Journal of Radiation Research*, vol. 62, no. 1, pp. 94–103, 2021. I
- [16] W. Zhu, Y. Huang, L. Zeng, X. Chen, Y. Liu, Z. Qian, N. Du, W. Fan, and X. Xie, "Anatomynet: deep learning for fast and fully automated whole-volume segmentation of head and neck anatomy," *Medical physics*, vol. 46, no. 2, pp. 576–589, 2019. I
- [17] D. Kawahara, M. Tsuneda, S. Ozawa, H. Okamoto, M. Nakamura, T. Nishio, A. Saito, and Y. Nagata, "Stepwise deep neural network (stepwise-net) for head and neck auto-segmentation on ct images," *Computers in Biology and Medicine*, vol. 143, p. 105295, 2022. I
- [18] T. Wang, Y. Lei, M. McDonald, J. J. Beitler, W. J. Curran, T. Liu, and X. Yang, "Multi-organ segmentation on head and neck dual-energy ct using deep neural networks," in *Medical Imaging 2021: Image*

Processing, vol. 11596. International Society for Optics and Photonics, 2021, p. 115961Y. I

[19] X. Dai, Y. Lei, T. Wang, J. Zhou, W. J. Curran, T. Liu, and X. Yang, “Deep attention mask regional convolutional neural network for head-and-neck mri multi-organ auto-delineation,” in *Medical Imaging 2021: Computer-Aided Diagnosis*, vol. 11597. International Society for Optics and Photonics, 2021, p. 115971B. I

[20] Y. Lei, J. Zhou, X. Dong, T. Wang, H. Mao, M. McDonald, W. J. Curran, T. Liu, and X. Yang, “Multi-organ segmentation in head and neck mri using u-faster-rcnn,” in *Medical Imaging 2020: Image Processing*, vol. 11313. International Society for Optics and Photonics, 2020, p. 113133A. I

[21] Y. Lei, J. Harms, X. Dong, T. Wang, X. Tang, S. Y. David, J. J. Beitler, W. J. Curran, T. Liu, and X. Yang, “Organ-at-risk (oar) segmentation in head and neck ct using u-rcnn,” in *Medical Imaging 2020: Computer-Aided Diagnosis*, vol. 11314. International Society for Optics and Photonics, 2020, p. 113144A. I

[22] S. Gou, N. Tong, S. Qi, S. Yang, R. Chin, and K. Sheng, “Self-channel-and-spatial-attention neural network for automated multi-organ segmentation on head and neck ct images,” *Physics in Medicine & Biology*, vol. 65, no. 24, p. 245034, 2020. I

[23] W. Chi, L. Ma, J. Wu, M. Chen, W. Lu, and X. Gu, “Deep learning-based medical image segmentation with limited labels,” *Physics in Medicine & Biology*, vol. 65, no. 23, p. 235001, 2020. I

[24] H. Kamezawa, H. Arimura, R. Yasumatsu, K. Ninomiya, and S. Haseai, “Radiomics-based malignancy prediction of parotid gland tumor,” in *International Forum on Medical Imaging in Asia 2019*, vol. 11050. SPIE, 2019, pp. 218–221. I

[25] Y. Dai, Y. Gao, and F. Liu, “Transmed: Transformers advance multi-modal medical image classification,” *Diagnostics*, vol. 11, no. 8, p. 1384, 2021. I

[26] H. Cao, Y. Wang, J. Chen, D. Jiang, X. Zhang, Q. Tian, and M. Wang, “Swin-unet: Unet-like pure transformer for medical image segmentation,” *arXiv preprint arXiv:2105.05537*, 2021. I, II-C

[27] O. Ronneberger, P. Fischer, and T. Brox, “U-net: Convolutional networks for biomedical image segmentation,” in *International Conference on Medical image computing and computer-assisted intervention*. Springer, 2015, pp. 234–241. II-A, IV-B

[28] J. Long, E. Shelhamer, and T. Darrell, “Fully convolutional networks for semantic segmentation,” in *Proceedings of the IEEE conference on computer vision and pattern recognition*, 2015, pp. 3431–3440. II-A

[29] K. Simonyan and A. Zisserman, “Very deep convolutional networks for large-scale image recognition,” *arXiv preprint arXiv:1409.1556*, 2014. II-A

[30] K. He, X. Zhang, S. Ren, and J. Sun, “Deep residual learning for image recognition,” in *Proceedings of the IEEE conference on computer vision and pattern recognition*, 2016, pp. 770–778. II-A

[31] A. Vaswani, N. Shazeer, N. Parmar, J. Uszkoreit, L. Jones, A. N. Gomez, Ł. Kaiser, and I. Polosukhin, “Attention is all you need,” *Advances in neural information processing systems*, vol. 30, 2017. II-B

[32] A. Dosovitskiy, L. Beyer, A. Kolesnikov, D. Weissenborn, X. Zhai, T. Unterthiner, M. Dehghani, M. Minderer, G. Heigold, S. Gelly *et al.*, “An image is worth 16x16 words: Transformers for image recognition at scale,” *arXiv preprint arXiv:2010.11929*, 2020. II-B

[33] Z. Liu, Y. Lin, Y. Cao, H. Hu, Y. Wei, Z. Zhang, S. Lin, and B. Guo, “Swin transformer: Hierarchical vision transformer using shifted windows,” in *Proceedings of the IEEE/CVF International Conference on Computer Vision*, 2021, pp. 10012–10022. II-B, III-E

[34] J. L. Ba, J. R. Kiros, and G. E. Hinton, “Layer normalization,” *arXiv preprint arXiv:1607.06450*, 2016. III-E

[35] Z. Zhou, M. M. Rahman Siddiquee, N. Tajbakhsh, and J. Liang, “Unet++: A nested u-net architecture for medical image segmentation,” in *Deep learning in medical image analysis and multimodal learning for clinical decision support*. Springer, 2018, pp. 3–11. IV-B

[36] T. Fan, G. Wang, Y. Li, and H. Wang, “Ma-net: A multi-scale attention network for liver and tumor segmentation,” *IEEE Access*, vol. 8, pp. 179 656–179 665, 2020. IV-B

[37] A. Chaurasia and E. Culurciello, “Linknet: Exploiting encoder representations for efficient semantic segmentation,” in *2017 IEEE Visual Communications and Image Processing (VCIP)*. IEEE, 2017, pp. 1–4. IV-B

[38] H. Zhao, J. Shi, X. Qi, X. Wang, and J. Jia, “Pyramid scene parsing network,” in *Proceedings of the IEEE conference on computer vision and pattern recognition*, 2017, pp. 2881–2890. IV-B

[39] H. Li, P. Xiong, J. An, and L. Wang, “Pyramid attention network for semantic segmentation,” *arXiv preprint arXiv:1805.10180*, 2018. IV-B

[40] L.-C. Florian and S. H. Adam, “Rethinking atrous convolution for semantic image segmentation,” in *Conference on Computer Vision and Pattern Recognition (CVPR). IEEE/CVF*, 2017. IV-B

[41] L.-C. Chen, Y. Zhu, G. Papandreou, F. Schroff, and H. Adam, “Encoder-decoder with atrous separable convolution for semantic image segmentation,” in *Proceedings of the European conference on computer vision (ECCV)*, 2018, pp. 801–818. IV-B



Yin Dai received the Ph.D. degree from the Department of Computer Science, Northeastern University, China, in 2015. She is currently an associate professor in the College of Medicine and Biological Information Engineering at Northeastern University, China. Her research lies at computer-aided diagnosis and medical image processing.



Sheng Liu is a master student from School and Hospital of Stomatology, China Medical University. He is majoring in Oral and Maxillofacial Surgery. Currently, he is mainly engaged in research on MRI, especially the application of MRI-Based radiomics features and machine learning in predicting lymph node metastasis in the oral squamous cell carcinoma.



Zi'an Xu is currently pursuing his master's degree in College of Medicine and Biological Information Engineering from Northeastern University, Shenyang, China. His research interests focus on deep learning in computer vision, classification and segmentation of medical images, and computer-aided diagnosis.



Lifu Shi received the Master degree from the Jilin University, China, in 2013. He is mainly researching in the field of data statistics and software science. In recent years, his research mainly focuses on big data analysis and data reconstruction in the field of magnetic medical detection and treatment such as magnetic particle imaging, homogeneous magnetic sensitivity immunoassay, etc., and also leading the development of several software systems for clinical diagnosis.



Fayu Liu Professor, Chief Physician, Doctoral Supervisor, Director of the Department of Oral and Maxillofacial Surgery, Oral Hospital of China Medical University. He is a member of the Standing Committee of Head and Neck Specialty Committee of China Medical Education Association; a member of Skull Base Surgery Branch of China Association for the Promotion of Healthcare International Exchange; a youth member of Oral and Maxillofacial-Head and Neck Tumor Specialty Committee of Chinese Oral Medical Association; a youth member of Head and Neck Tumor Specialty Committee of Chinese Anti-Cancer Association. He has been engaged in clinical, teaching and research work in oral and maxillofacial-head and neck surgery. He has received a Research Fellowship from Sloan-Kettering Cancer Center, Roswell Park Cancer Center and the State University of New York at Buffalo, and has led one National Natural Science Foundation, four provincial-level projects, two municipal-level projects, and participated in one national key research and development project. He has published 20 papers in foreign SCI journals and many papers in domestic core journals as the first author or corresponding author. He participated in writing the book "Repair and Reconstruction of Head and Neck Defects" published by People's Health Publishing House, and won one second prize and two third prizes of Science and Technology Progress of Liaoning Provincial Government.



Jun Fu received the Ph.D. degree in mechanical engineering from Concordia University, Montreal, QC, Canada, in 2009. He was a Postdoctoral Fellow/ Associate with the Department of Mechanical Engineering, Massachusetts Institute of Technology, Cambridge, MA, USA, from 2010 to 2014. He is currently a Full Professor with Northeastern University, Shenyang, China. He has authored/coauthored more than 70 publications, which appeared in journals, conference proceedings, and book chapters. His current research interests include switched systems, robust control, mathematical programming, and dynamic optimization. Dr. Fu received the 2016 Young Scientist Award from the Chinese Association of Automation. He is currently an Associate Editor of the IEEE TRANSACTIONS ON SYSTEMS, MAN, AND CYBERNETICS: SYSTEMS, IEEE TRANSACTIONS ON NEURAL NETWORKS AND LEARNING SYSTEMS, Control Engineering Practice (IFAC), and Journal of Industrial and Management Optimization.



Siqi Li graduated from the Department of Oromaxillofacial-Head and Neck Surgery, School of Stomatology of China Medical University with a master's degree in 2021. Now work in the Department of Stomatology, the children's hospital, ZheJiang University School of Medicine. Research interest: parotid gland tumors and radiomics.